The 1.9 Å Resolution Crystal Structure of Phosphono-CheY, an Analogue of the Active Form of the Response Regulator, CheY † , ‡

ARTICLE *in* BIOCHEMISTRY · JUNE 2000

Impact Factor: 3.02 · DOI: 10.1021/bi9925524 · Source: PubMed

6 AUTHORS, INCLUDING:

Chris Halkides
University of North Carolina at Wilmington
38 PUBLICATIONS **620** CITATIONS
SEE PROFILE

Megan M Mcevoy
The University of Arizona
36 PUBLICATIONS **1,049** CITATIONS
SEE PROFILE

Frederick W Dahlquist
University of California, Santa Barbara
223 PUBLICATIONS **10,503** CITATIONS
SEE PROFILE

The 1.9 Å Resolution Crystal Structure of Phosphono-CheY, an Analogue of the Active Form of the Response Regulator, CheY[†,‡]

Christopher J. Halkides,[§] Megan M. McEvoy,[||] Eric Casper,[§] Philip Matsumura,[⊥] Karl Volz,*[,⊥] and Frederick W. Dahlquist*[,||]

Department of Chemistry, University of North Carolina at Wilmington, Wilmington, North Carolina 28403-3297, Department of Microbiology and Immunology (M/C 790), E-704 Medical Sciences Building, 835 South Wolcott Avenue, University of Illinois at Chicago, Chicago, Illinois 60612, and Department of Chemistry, The Institute of Molecular Biology, University of Oregon, Eugene, Oregon 97403-1229

Received November 4, 1999; Revised Manuscript Received February 22, 2000

ABSTRACT: To structurally characterize the activated state of the transiently phosphorylated signal transduction protein CheY, we have constructed an α-thiophosphonate derivative of the CheY D57C point mutant and determined its three-dimensional structure at 1.85 Å resolution. We have also characterized this analogue with high-resolution NMR and studied its binding to a peptide derived from FliM, CheY's target component of the flagellar motor. The chemically modified derivative, phosphono-CheY, exhibits many of the chemical properties of phosphorylated wild-type CheY, except that it is indefinitely stable. Electron density for the α-thiophosphonate substitution is clear and readily interpretable; omit refinement density at the phosphorus atom is greater than 10σ. The molecule shows a number of localized conformational changes that are believed to constitute the postphosphorylation activation events. The most obvious of these changes include movement of the side chain of the active site base, Lys 109, and a predominately buried conformation of the side chain of Tyr 106. In addition, there are a number of more subtle changes more distant from the active site involving the α4 and α5 helices. These results are consistent with our previous structural interpretations of other CheY activation mutants, and with our earlier hypotheses concerning CheY activation through propagation of structural changes away from the active site.

Two component systems are ubiquitous in prokaryotes and lower eukaryotes (*1*−*3*). Virtually all physiological responses to environmental signals are mediated by these systems. Each two-component system is composed of at least one sensor kinase and one accompanying cognate response regulator. *Escherichia coli* contains ∼30 pairs of kinases/response regulators, and more than 300 of these systems have been described (*4*). Although the response regulators of two-component systems share overall structural similarity (*5*), these systems are remarkable in their specificity.

CheY, a response regulator from the bacterial chemotaxis pathway, is the most thoroughly studied of the response regulators of two-component families. When Asp 57 becomes phosphorylated (*6*), CheY switches from an inactive conformation to an active form, CheY-P. Yet since the half-life of CheY-P is so short (∼20 s), all structure−function studies to date have been on the unphosphorylated forms. To further understand the activation process of CheY, we have prepared a stably phosphonomethylated form of CheY D57C (*7*). We previously reported that this analogue of CheY-P, called phosphono-CheY, exhibits many of the properties of CheY-P, including an increased level of binding to the flagellar motor component FliM and to the protein which accelerates dephosphorylation of CheY-P, CheZ (*7*).

In this paper, we show that the multidimensional NMR spectrum of phosphono-CheY has a chemical shift pattern along its sequence that has features in common with that of CheY-P. The phosphonomethyl group is clearly revealed in the high-resolution crystal structure. The presence of the phosphonomethyl group results in the movement of several side chains; however, there is only one area of relatively modest displacement of the backbone relative to CheY. We conclude that activation as mimicked by phosphono-CheY does not involve large-scale conformational changes but rather occurs via the motions of several side chains and possibly the backbone near residue 90.

MATERIALS AND METHODS

Protein Modification and Purification. Synthesis and purification of phosphono-CheY were carried out as previously described (*7*). Fluorimetric titration of phosphono-CheY was performed with sample conditions, instrument parameters, and data analysis as previously described (*8*) with the following modifications. Phosphono-CheY at a concentration of 10 μM in a total volume of 2 mL was titrated with 5 μL additions of 10 mM FliM peptide from 0 to 338.2 μM

[†] This work was supported by National Institutes of Health Grants AI18985 (to P.M.), GM47522 (to K.V.), and AI17808 (to F.W.D.).

[‡] Atomic coordinates and structure factors have been deposited in the Protein Data Bank, accession code 1C4W.

* To whom correspondence should be addressed. K.V.: e-mail, karl@e002.mim.uic.edu. F.W.D.: e-mail, fwd@morel.uoregon.edu.

[§] University of North Carolina at Wilmington.

[||] University of Oregon.

[⊥] University of Illinois at Chicago.

10.1021/bi9925524 CCC: $19.00
Published on Web 04/13/2000

FliM peptide. CheY D13K/Y106W at a concentration of 5.6 μM in a total volume of 50 μL was titrated with 0.5 μL additions of 10 mM FliM peptide from 0 to 825.7 μM FliM peptide.

NMR Data Collection and Analysis. $^1H-^{15}N$ spectra of phosphono-CheY in 50 mM MOPS at pH 6.9 were acquired at 600 MHz with a Varian INOVA spectrometer at 25 °C. HSQC, TOCSY-HSQC, and NOESY-HSQC spectra were acquired with sensitivity enhancement and selection of coherences using gradients (*9*). For the NOESY-HSQC experiments, we acquired 8 scans of 512 complex points in the observe dimension (sw = 8000 Hz), 128 complex points in the ^1H dimension (sw = 8000 Hz), and 64 complex points in the ^{15}N dimension (sw = 2000 Hz). The mixing time was 100 ms, and the total acquisition time was about 3.5 days. For the TOCSY-HSQC experiment, we acquired 16 scans of 512 points in the observe dimension (sw = 8000 Hz), 128 points in the ^1H dimension (sw = 8000 Hz), and 32 points in the ^{15}N dimension (sw = 2000 Hz). Referencing was accomplished by setting the resonance of Gly 52 to 105.6 ppm in the ^{15}N dimension (*10*) and by setting the center of the spectrum to 4.8 ppm in both ^1H dimensions. Data were processed with FELIX 95 (Biosym/Molecular Simulations).

Crystallization, Data Collection, and Processing. Small, needle-like crystals were grown using the hanging drop method in 28% PEG 6000, 200 mM sodium acetate, and 100 mM PIPES (pH 6.9). Large bipyramidal crystals of tetragonal phosphono-CheY were also grown in ~1.8 M ammonium sulfate, but these crystals typically diffracted only to ~4 Å. The needle form of phosphono-CheY had the same space group and packing as orthorhombic wild-type CheY, $P2_12_12_1$, with the following room-temperature unit cell dimensions: $a = 45.9$ Å, $b = 49.3$ Å, and $c = 54.0$ Å. The a and c values were identical to those of wild-type CheY, but b was larger by 4.9%. Diffraction data were collected under cryoconditions at beamline 9-1 of the Stanford Synchrotron Radiation Facility at a wavelength of 0.98 Å. The crystal was transferred successively into solutions containing buffer, PEG 6000, and 5, 10, 15, and finally 20% glycerol over a few minutes, and then immersed in liquid nitrogen. Data were recorded on a 345 mm diameter MAR detector at a crystal-to-detector distance of 150 mm, with a zero 2θ offset position for a theoretical upper resolution limit of 1.84 Å. The crystal was exposed for a total of ~3 h for two scans: first, a scan of 40 frames, at 60 s per frame, in 2.5° increments for a total of 100°, followed by a shorter scan of 45° in 2.5° increments, at 60 s per frame, at a χ offset of 90° using an extended-arc goniometer head from Charles Supper Co. Data processing and reduction were carried out using the DENZO and SCALEPACK program packages (*11*). The final data set included a total of 84 092 observations of 10 492 unique reflections, with an unweighted absolute R-factor on intensities of 7.4%. Statistics for the final data set used in the structural solution are given in Table 1.

Phasing and Structural Refinement. Even though the phosphono-CheY crystals were not closely isomorphous with those of wild-type CheY, the initial phasing attempt of the phosphono-CheY structure was successful with X-PLOR (*12*) using the wild-type structure with all solvent molecules excluded, no rotamers, and residue 57 modeled as an alanine. The R-factor fell from 48.2 to 31.0%. The original wild-type model was then least-squares superimposed onto the X-PLOR results, and refinement of its atomic positions was resumed using the restrained least-squares method (*13*). The α-thiophosphonate moiety was never included in the refinement. The R-factor converged to a final value of 20.8% after a total of 29 rounds of refinement, interspersed with partial rebuilds. Reflections (9653) greater than 2σ in the resolution range of 10−1.85 Å were used in the last refinement cycle. The final refinement status is presented in Table 2.

Table 1: Statistics for Data and Final Refinement of Phosphono-CheY from *E. coli*

resolution limit (Å)	no. of predicted reflections	% complete	% > $2\sigma_F$	refinement R value (%)[a]
$\infty \rightarrow 10.00$	89	100	–	–
$10.00 \rightarrow 3.58$	1515	95.2	95.1	22.2
$3.58 \rightarrow 2.85$	1507	94.1	93.2	20.6
$2.85 \rightarrow 2.48$	1537	95.3	92.7	20.6
$2.48 \rightarrow 2.25$	1514	95.6	92.3	20.8
$2.25 \rightarrow 2.09$	1474	94.4	89.1	20.7
$2.09 \rightarrow 1.96$	1591	93.8	85.0	20.8
$1.96 \rightarrow 1.85$	1699	94.1	77.6	20.8
$10.00 \rightarrow 1.85$	10837	93.9	88.3	20.8

[a] $R = [(\sum|F_o - F_c|)/(\sum|F_o|)] \times 100$.

Table 2: Refinement Restraints and Root-Mean-Square Deviations from Ideal of Chemically Modified *E. coli* CheY Mutant D57C Using 9653 Reflections from 10 to 1.85 Å

parameter	target σ	final value
distance restraints		
bond distance	0.020	0.020
angle distance	0.040	0.043
planar distance	0.050	0.051
plane restraint (Å)	0.020	0.012
chiral-center restraint (Å^3)	0.150	0.174
nonbonded contact restraints (Å)		
single torsion contact	0.500	0.178
multiple torsional contact	0.500	0.227
possible hydrogen bond	0.500	0.247
conformational torsion angle restraint (deg)		
planar (ω, 0°, 180°)	3.0	2.1
staggered (±60°, 180°)	15.0	16.3
orthonormal (±90°)	20.0	24.6
isotropic thermal restraints (Å^2)		
main chain bond	1.000	0.991
main chain angle	1.500	1.614
side chain bond	1.000	1.196
side chain angle	1.500	1.959
X-ray	$0.7\langle\|F_o - F_c\|\rangle$	20.79%

Calculations of electron density maps and other data processing were carried out with the XTAL (*14*) and CCP4 (*15*) software packages, and several other locally developed programs. The least-squares refinement was carried out with the software packages PROTIN (*13*) and PROFFT (*16*). Visualization of the electron density maps and model rebuilding were carried out using the graphics package QUANTA on a Silicon Graphics Indigo system.

RESULTS AND DISCUSSION

Signaling Properties of Phosphono-CheY. We have recently described a quantitative fluorescence-based binding assay for CheY derivatives to the downstream targets of CheY-P, including the flagellar switch protein, FliM (*8*). This approach uses a peptide corresponding to the 16 N-terminal

residues of FliM (*17*). Interestingly, this peptide binds to CheY-P with nearly the same affinity as intact FliM and seems to exhibit a similar modulation of affinity with phosphorylation. This approach provides a more quantitative way to compare the properties of phosphono-CheY to other CheY derivatives than we previously published (*7*). We summarize below the results obtained with the binding of the FliM-derived peptide to CheY, CheY-P, phosphono-CheY, and the double mutant CheY D13K/Y106W that generates tumbly swimming behavior in the absence of phosphorylation (*18*). There is an approximate 25-fold increase in the affinity of the peptide for CheY-P as compared to that for CheY. The dissociation constant of the peptide for CheY-P is 27 ± 1 μM. Phosphono-CheY binds about 3-fold less tightly (73 ± 6 μM), while the double mutant binds about 5-fold less well than CheY-P (150 ± 16 μM). Thus, phosphono-CheY binds more tightly than the double mutant and in that sense is a better analogue of CheY-P than the double mutant. These results differ somewhat from the results of Scharf et al. Using a cross-linking assay, they observed that the double mutant interacted with FliM about 80% as well as the phosphorylated wild-type CheY (*18*). Our equilibrium assays of binding are more easily interpreted in a quantitative sense than are the cross-linking experiments; however, the cross-linking experiments were carried out with an intact version of FliM. It is possible that some part of FliM other than the peptide sequence interacts with the activated forms of CheY.

It is clear that the double mutant can generate tumbly swimming, while the signaling behavior of phosphono-CheY is less obvious. Using assays with bacterial envelopes, we have not been able to observe the clockwise (CW) flagellar rotation characteristic of tumbly swimming when phosphono-CheY is introduced into permeablized bacterial cells (M. Eisenbach, A. Bren, C. J. Halkides, and F. W. Dahlquist, unpublished). However, these assays are very complicated, and a negative result is difficult to interpret. One possibility is that phosphono-CheY can bind to the flagellar switch but does not induce the conformational change in the flagellar apparatus needed to cause a switch in the sense of rotation. Alternatively, there could be additional role(s) for CheY or CheY-P needed to induce CW rotation that are not yet understood, and phosphono-CheY does not satisfy these unknown functions.

^{1}H and ^{15}N NMR. The chemical shift changes in CheY caused by phosphorylation have been previously identified by multidimensional NMR spectroscopy (*10*). The largest chemical shift changes were observed in residues close to Asp 57, the site of phosphorylation, and other changes were observed more globally (*10*). These results suggested that a conformational change propagates from Asp 57 to the C-termini of the other β-strands. A similar set of differences in chemical shifts is observed when phosphono-CheY is compared with unphosphorylated CheY (Figure 1a), although some resonances corresponding to residues near the phosphono group are missing, most likely due to conformational exchange. The regions of the protein which exhibit the greatest combined (^{1}H and ^{15}N) chemical shifts for amide protons are similar, suggesting that phosphonomethylation and phosphorylation bring about similar conformational changes. Note that the comparisons with phosphono-CheY

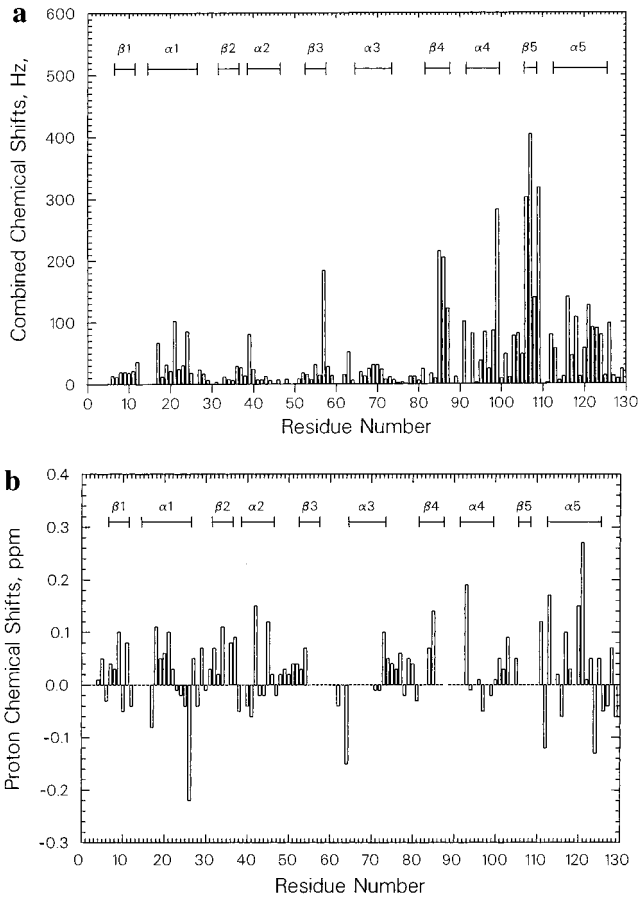

FIGURE 1: (a) Combined chemical shift differences of phosphono-CheY compared to wild-type CheY as a function of residue number. Twenty residues (16%) of phosphono-CheY could not be assigned. (b) Proton chemical shift differences of phosphono-CheY compared to CheY-P as a function of residue number. Eighty-seven residues (68%) have assignments for both phosphono-CheY and CheY-P.

were carried out in the absence of magnesium ion while the phosphorylation comparisons were carried out in the presence of magnesium ion. We used a combined shift of 74 Hz to define a "significant shift" in our comparison of the resting and phosphorylated states of CheY, placing residues 17, 21, 23, 39, 57, 59, 60, 63−69, 85−88, 94, 107, 112, 116, 118, 121−124, and 126 in this category. Using the same criterion, we see significant shifts in phosphono-CheY in residues 21, 24, 39, 57, 85−87, 91, 93, 96, 98, 99, 103, 104, 106−109, 112, 116, 118, 121−124, and 126. There are nine residues that are members of both lists (21, 39, 57, 85−87, 107, 112, and 121). However, as shown in Figure 1b, a detailed comparison of proton chemical shifts shows that there are significant differences in the environment of the backbone amides in the two cases. We conclude that there are structural changes introduced in similar regions by phosphorylation and by the introduction of the phosphono moiety but that the details of these structural changes are somewhat different in the two cases.

General Description of Crystallographic Results. The electron density maps from the final $|2F_o - F_c|$, α_{calc} and $|F_o - F_c|$, α_{calc} difference Fourier calculations are clear and well-defined for the entire backbone of the molecule. The average thermal parameter for all protein atoms is 21.7 Å^2. The variation of thermal parameters throughout the phosphono-CheY molecule is very similar to that for wild-type CheY. The final coordinate set consists of 1121 atoms, of which

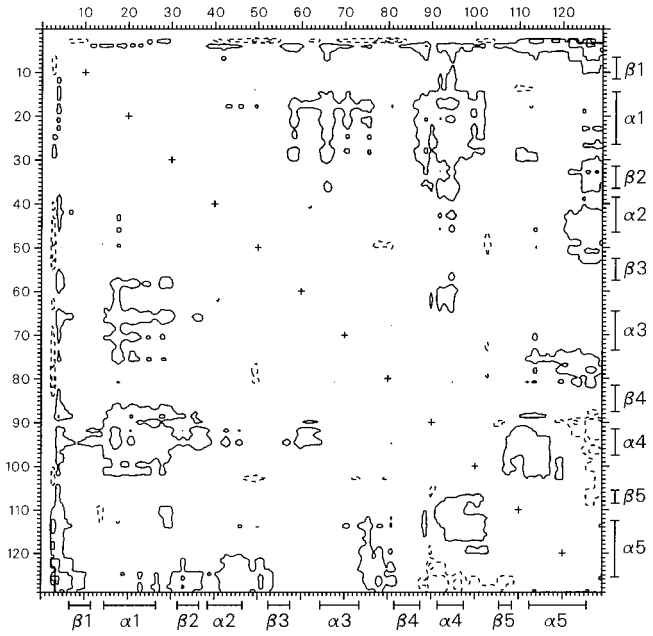

FIGURE 2: δ−distance plot of Cα atoms of wild-type CheY compared to phosphono-CheY. Contour levels start at the ±0.4 Å level and proceed in ±0.4 Å intervals. Solid contours correspond to regions of contraction in the phosphono-CheY molecule relative to the wild type, and dashed contours indicate expansion. The largest differences are in the 90's loop, α4, and the C-terminus at the end of α5.

981 are protein and 140 are solvent with unit occupancies. The α-thiophosphonate was never modeled in the refinement calculations (residue 57 was treated as an alanine). Only one side chain, that of Asn 23, was modeled and refined as a rotamer.

Overall Comparison of Wild-Type CheY with Phosphono-CheY. The δ−distance plot (Figure 2) provides an unbiased comparison of wild-type (Mg^{2+}-free) CheY with phosphono-CheY. Since the two forms of CheY crystallized in the same space group, the intermolecular contacts are essentially the same; therefore, any differences shown by the δ−distance plot most likely represent changes caused by the D57C mutation and the phosphonomethylation of Cys 57. A region of the protein beginning at the C-terminus of β4 and continuing well into α4 shows a significant contraction-type repositioning with respect to the remainder of the molecule. These overall structural differences are greater than those between the weakly activating D13K mutant and wild-type CheY (*19*).

A least-squares superposition of the two structures suggests that some of the observed differences between phosphono-CheY and wild-type CheY are the result of random error, while other changes are significant (Figure 3). The overall average rms difference is 0.40 Å, which is about the same as the difference when two molecules of the CheY mutant T87I within an asymmetric unit were compared with each other, 0.38 Å (*20*). However, a comparison of the δ−distance plot of molecule A versus B of CheY T87I (*20*) with the plot of phosphono-CheY versus CheY (Figure 2) suggests that some differences in the latter are in fact significant. The T87I A versus B plot does not have distinct, sharp peaks, whereas the CheY versus phosphono-CheY plot does. Moreover, the changes in the phosphono-CheY structure are larger in the C-terminal than the N-terminal half of the

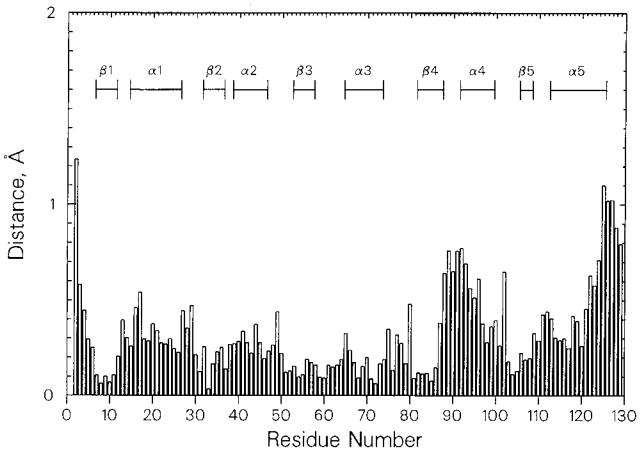

FIGURE 3: Plot of rms differences between Cα positions of phosphono-CheY and wild-type CheY molecules after least-squares superposition. The average rms difference for all α-carbon atoms is 0.40 Å.

protein, and are largest near residue 90 (∼1 Å). Indeed, when only residues 5−50 (the portion of the two molecules showing the least change in the δ−distance plot) are used to superimpose the two structures, the rms differences near residue 90 become larger.

The region near residue 90, which encompasses the latter portion of β4, the β4−α4 loop, and a portion of α4, is implicated by mutagenesis and by chemical shift changes as being a critical part of the activating conformational change. In particular, the CheY mutant I95V exhibits a hyperactive phenotype that depends on phosphorylation (*21*), whereas the T87I mutant confers a smooth-swimming phenotype (*20*). Both Thr 87 and Ala 88 are highly conserved (*5*), and Val 86 and Ala 88 both exhibit large chemical shift changes upon phosphorylation (*10*).

The rms differences between phosphono-CheY and CheY (Figure 3) are greater than the differences between CheY mutant D13K and CheY, 0.4 versus 0.21 Å. CheY D13K gives a CW bias in a phosphorylation-independent manner, but this mutant exhibits little affinity for FliM or CheZ (*21*−*23*). In contrast, phosphono-CheY binds FliM and CheZ much better than unphosphorylated, wild-type CheY (*7*).

The most significant differences between phosphono-CheY and wild-type CheY occur in two regions. The first begins at Thr 87 and extends to Gly 102; this region corresponds to the loop between β4 and α4 (the "90's loop") plus helix α4. The second extends from Leu 120 to the C-terminus, corresponding to the last half of helix α5. The largest differences are ∼1 Å, which are 5-fold greater than the rms differences in the first two-thirds of the molecules. These two regions are also altered in mutants of CheY such as T87I (*20*). While this region may be more susceptible to structural deformation, it is more likely that the differences represent a functionally important conformational change. In the response regulator NtrC, for example, mutations at positions 86 and 89, which are in helix α4, lead to a constitutively active phenotype (*24*). Similar changes in phenotype have been seen in point mutants of other response regulators (*5*).

Structure at the Active Site. The $|F_o - F_c|$, α_{calc} difference Fourier electron density at position 57 is easily interpretable as an α-thiophosphonate, confirming the chemical modification (Figure 4). The density for the side chain bifurcates

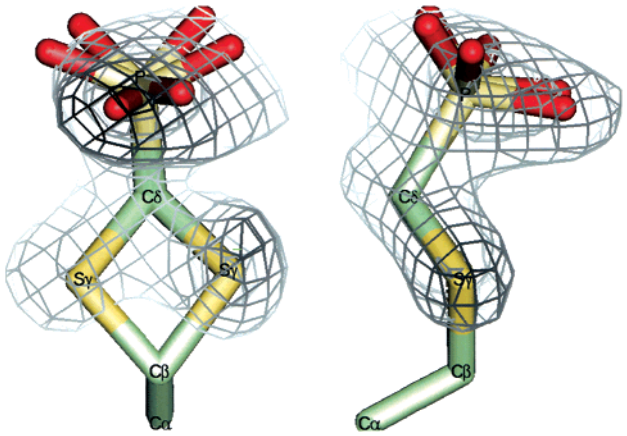

FIGURE 4: Two perpendicular views of the final $|F_o - F_c|$, α_{calc} electron density in the active site from omit refinement of phosphono-CheY, in which residue 57 was modeled as an alanine. The map is contoured at 3.5σ and 7σ. Two idealized models of an α-thiophosphonate group have been manually positioned into the density. Two distinct rotameric positions are observed for the sulfur atoms of the α-thiophosphonate, although the phosphorus and carbon atoms occupy essentially identical positions. The six oxygen positions are simply the result of positioning each of the two idealized models with an oxygen atom trans to its Sγ atom.

between the Cβ and Cδ positions, showing that the Sγ atom of the Cys 57 side chain clearly exists in two rotameric conformations ($\chi_1 = -95$ and 180°). The interconversion of these two conformations may result in broadening on the NMR chemical shift time scale (see above). Electron density at the position of the phosphorus atom reaches the 10σ level. The electron density of the phosphoryl group appears to be rounded and rotationally disordered; the group may have true disorder, or the individual oxygen atoms simply may not be resolvable at this resolution.

A sphere of very well-defined electron density resides in the Mg^{2+} binding position in the active site, coordinated by Asp 13, the carbonyl oxygen of Asn 59, and a solvent molecule. This density has been modeled as solvent, and refines to become the solvent molecule with the lowest temperature factor. The three bonds to it described above are short, an average of 2.4 Å in length. These distances are too short for hydrogen bonds of water molecules, but still too long for a Mg^{2+} ion. The center of density is also ~2.9 Å from the cluster of oxygen atoms in the phosphoryl group. It is probable that this density arises from a sodium ion residing in the divalent cation binding site. This structure was determined in the absence of added magnesium ion so it is possible that magnesium ion would normally be present at this site.

The side chain of Lys 109 has a reasonable folded conformation ($\chi_{1-4} = 79$, 85, 174, and 100°, respectively), and the ϵ-amino group has hydrogen bonding contacts (~3 Å) with the oxygen atoms of the phosphonate group (Figure 5). This conformation is markedly different from that of the fully extended conformation in wild-type CheY, ($\chi_{1-4} = 69$, −178, 173, and −174°, respectively), showing that it is the χ_2 and χ_4 angles that bend to accommodate the bulk of the α-thiophosphonate. It does not appear that structural changes propagate directly from the side chain of Lys 109 through its backbone to the rest of the molecule; the global effects are more subtle, as discussed above.

The combined effects of the negative charges on the phosphoryl group oxygen atoms and the movement of the positively charged ϵ-amino group of Lys 109 by ~3.5 Å may be important for the binding of CheZ and FliM by electrostatic contacts to these groups. The fact that the CheY mutant D57E does not show enhanced binding to FliM (*25*) may be explained by several factors: the difference in the position and geometry of the negative charges between phosphono-CheY and CheY D57E and the ability of the phosphoryl group to attain between one and two negative charges, depending on pH.

Finally, the side chain of Asn 59 assumes a χ_1 position that orients it farther away from the site of phosphorylation in phosphono-CheY (Figure 5). It is unknown whether this has functional significance, but it may partly explain the large NMR shifts upon phosphorylation seen for Asn 59 and its neighbor Gly 65, a highly conserved residue (*5*, *10*).

Significant Differences Remote from the Active Site. Besides the obvious substitution at the active site, the only other significant difference between wild-type CheY and phosphono-CheY was the position of the side chain of Tyr 106. In wild-type CheY, Tyr 106 is a rotamer, occupying two very different positions: one internal, solvent-inaccessible and the other external, totally exposed to solvent. In the phosphono-CheY structure, the electron density shows that Tyr 106 is exclusively in the internal position (Figure 6). We interpret this restriction of rotameric positioning solely as a result of the phosphonomethyl group substitution on the molecule, and we propose that this same effect occurs in CheY-P. The importance of the rotameric state of Tyr 106 has been inferred from previous structure−function studies on five inactive and hyperactive mutants: T87I (*20*), Y106W (*26*), T87I/Y106W (*26*), T87S (X. Zhu, P. Matsumura, and K. Volz, manuscript in preparation), and Y106F (X. Zhu, P. Matsumura, and K. Volz, manuscript in preparation).

Conclusions and Mechanism for CheY Activation and Signaling. These NMR and crystallographic results on phosphono-CheY provide a good basis for constructing a model of the activated, signaling form of CheY. The activation scenario begins with phosphorylation at Asp 57. Phosphorylation changes the surface topology and electrostatics at the phosphoryl group, as well as Lys 109. The solvent structure is also rearranged at the active site. The movement of Lys 109 permits a slight shift in the position of helix α5 and the loop leading into it from Lys 109. Our view of this motion may reflect the absence of added magnesium ion, a requirement for crystallization. The presence of a bound magnesium ion in this region could change the details of electrostatic environment and the resulting structure. However, since magnesium ion is not present in our binding studies with the FliM peptide, the structural changes we observe reflect the increased level of activation that is observed. The change in the solvent structure propagates to the channel region near Thr 87. This rearrangement increases the propensity for the Tyr 106 side chain to adopt its internal conformation, significantly changing the contour and H-bonding capacity at the surface near residue 106. In the complex between CheY and the P2 domain of CheA, the side chain of Tyr 106 is held in the external conformation (*27*, *28*) by a hydrogen-bonded interaction of the tyrosine side chain hydroxyl with His 181

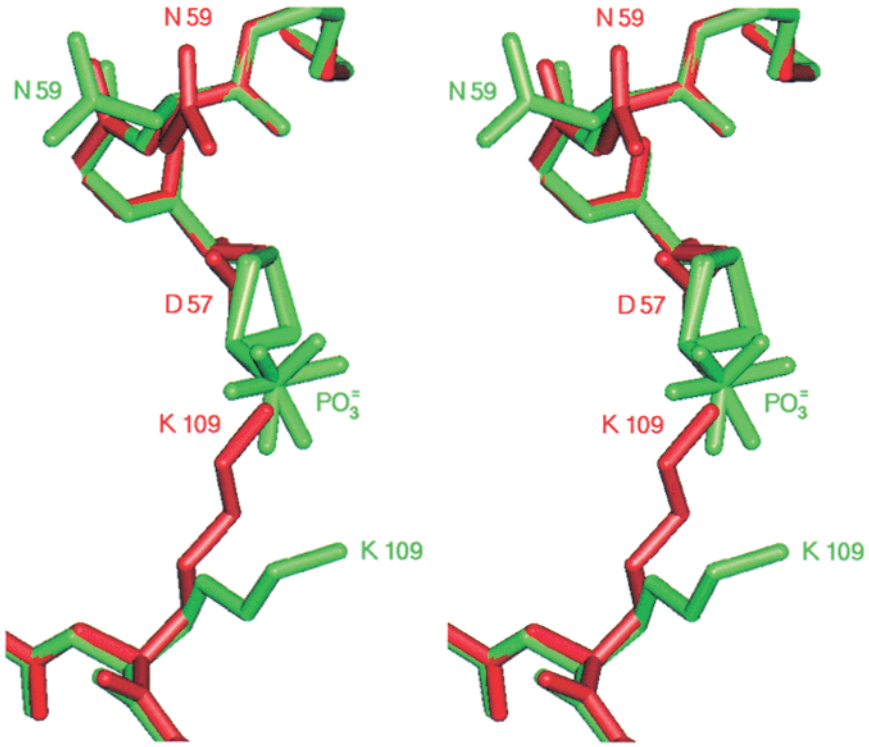

FIGURE 5: Stereodiagram comparing phosphono-CheY (green) and wild-type CheY (red) in the active site. The phosphoryl group has a charge−charge interaction with the ϵ-amino group of Lys 109, which has been displaced by 3.5 Å to accommodate this moiety.

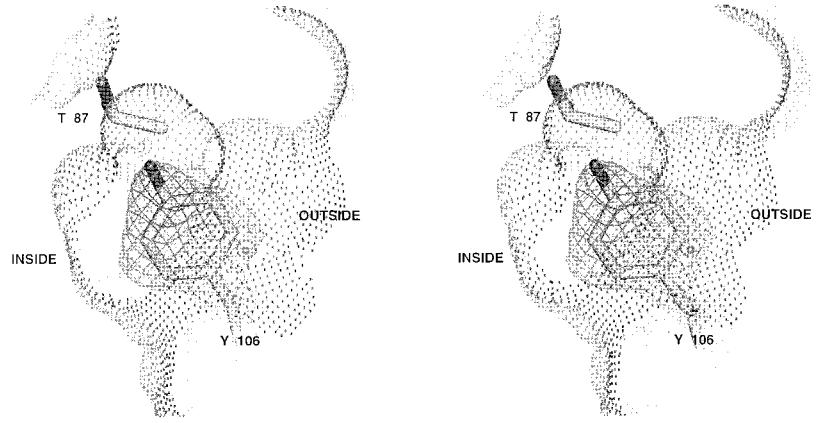

FIGURE 6: Stereodiagram of final $|F_o - F_c|$, α_{calc} omit map electron density for residue 106 of phosphono-CheY, contoured at 3.5 σ. Residue 106 was modeled as a glycine. The solvent accessible surface was also calculated with a glycine at position 106 for visualization of the internal cavity. The Tyr 106 side chain occupies only the internal, solvent-inaccessible position. Compare this figure to Figure 4 of Zhu et al. (*25*).

in CheA. The switch of Tyr 106 to the inside would break this interaction and could readily explain the decrease in affinity for CheA that is observed when CheY is phosphorylated (*29*).

Recently, several structures of phosphorylated forms of response regulator domains have been reported [FixJ (*30*), Spo0A (*31*), and NtrC (*32*)]. The structures of the phosphorylated and unphosphorylated forms of FixJ are currently the most complete high-resolution structures that directly compare the two forms. These structures show changes propagating from the site of phosphorylation to the homologue of Tyr 106, Phe 101, moving that residue from a solvent-exposed to interior position. These changes are accompanied by the motion of the Thr 87 homologue (Thr 82) toward the active site. A similar argument has been presented for the activation of Spo0A by Lewis et al. (*31*), although they lack a structure of the resting form of the protein. Our work shows no significant movement of Thr 87, yet Tyr 106 moves to the inside. We conclude that the motion of Thr 87 is not a required feature of response regulator activation.

The changes associated with the repacking near the active site cause a repositioning of the 90's loop and helix α4. Collectively, all of these topological changes in the α4−β5−α5 region (the FliM-binding surface) have transformed CheY into its signaling conformation, and the affinity for CheA is lowered while that for FliM is increased (*33*). It is not clear that phosphono-CheY can produce the CW signaling state in the flagellar assembly. It has been suggested that CheY-P likely stabilizes the CW form of the flagellar assembly by binding to the CW form with somewhat higher affinity than it does to the counterclockwise (CCW) form

(*34*, *35*). In this view, certain nonphosphorylatable mutants of CheY, such as the mutant CheY D13K, have the ability to differentially bind to the CW form but do so with a lower affinity than CheY-P. Thus, switching to the tumbly state is only observed at high levels of expression of these variants. In the case of phosphono-CheY, the affinity for FliM is high, but it is possible that phosphono-CheY does not properly distinguish the CW and CCW forms.

The structural changes we observe away from the active site are more subtle than those seen in FixJ (*30*) and NtrC (*32*). In FixJ, phosphorylation induces large changes in the loop than connects β4 and α4, resulting in backbone motions of up to 6 Å and smaller shifts in the loop connecting β1 and α1. In NtrC, there are significant changes involving α3−β5 and a rather drastic register shift in α4 that results in the exposure of a hydrophobic surface involving residues in that helix. Thus, it appears that phosphorylation of the various response regulator domains initiates similar events, and all likely share the conversion of the homologues of Tyr 106 from a solvent-exposed to a more internal position. This, in turn, results in a different reorganization of the packing of the secondary structure elements of each response regulator domain and generates the necessary structural change for each system. The bulk of these changes are seen in the C-terminal half of the various response regulators. Thus, the family of response regulator domains appear to represent a highly adaptable functional unit that exploits a common mechanism of conformational change near the active site to produce different changes at more distant parts of the protein.

ACKNOWLEDGMENT

We thank the staff at beamline 9-1 of the Stanford Synchrotron Radiation Laboratory (SSRL) for use of their facilities. SSRL is funded by the Department of Energy, Office of Basic Energy Sciences. The Biotechnology Program at SSRL is supported by the National Institutes of Health, National Center for Research Resources, Biomedical Technology Program, and the Department of Energy, Office of Biological and Environmental Research.

REFERENCES

1. Hoch, J. A., and Silhavy, T. J. (1995) *Two-Component Signal Transduction*, ASM Press, Washington, DC.
2. Parkinson, J. S. (1993) *Cell 73*, 857−871.
3. Parkinson, J. S., and Kofoid, E. S. (1992) *Annu. Rev. Genet. 26*, 71−112.
4. Goudreau, P., and Stock, A. M. (1998) *Curr. Opin. Microbiol. 1*, 160−169.
5. Volz, K. (1993) *Biochemistry 32*, 11741−11753.
6. Sanders, D. A., Gillece-Castro, B. L., Stock, A. M., Burlingame, A. L., and Koshland, D. E., Jr. (1989) *J. Biol. Chem. 264*, 21770−21778.
7. Halkides, C. J., Zhu, X., Phillion, D. P., Matsumura, P., and Dahlquist, F. W. (1998) *Biochemistry 37*, 13674−13680.
8. McEvoy, M. M., Bren, A., Eisenbach, M., and Dahlquist, F. W. (1999) *J. Mol. Biol. 289*, 1423−1433.
9. Zhang, O., Kay, L. E., Olivier, J. P., and Forman-Kay, J. D. (1994) *J. Biomol. NMR 4*, 845−858.
10. Lowry, D. F., Roth, A. F., Rupert, P. B., Dahlquist, F. W., Moy, F. J., Domaille, P. J., and Matsumura, P. (1994) *J. Biol. Chem. 269*, 26358−26362.
11. Otwinowski, Z., and Minor, W. (1997) *Methods Enzymol. 276*, 307−326.
12. Brunger, A. T., and Rice, L. M. (1997) *Methods Enzymol. 277*, 243−268.
13. Hendrickson, W. A. (1985) *Methods Enzymol. 115*, 252−270.
14. Hall, S. R., King, G. S. D., and Stewart, J. M. (1988) *XTAL2.4 User's Manual*, Universities of Western Australia and Maryland, Perth, Australia.
15. Dodson, E. J., Winn, M., and Ralph, A. (1997) *Methods Enzymol. 277*, 620−633.
16. Finzel, B. F. (1987) *J. Appl. Crystallogr. 20*, 53−55.
17. Bren, A., and Eisenbach, M. (1998) *J. Mol. Biol. 278*, 507−514.
18. Scharf, B. E., Fahrner, K. A., Turner, L., and Berg, H. C. (1998) *Proc. Natl. Acad. Sci. U.S.A. 95*, 201−206.
19. Jiang, M., Bourret, R., Simon, M. I., and Volz, K. (1997) *J. Biol. Chem. 272*, 11850−11855.
20. Ganguli, S., Wang, H., Matsumura, P., and Volz, K. (1995) *J. Biol. Chem. 270*, 17386−17393.
21. Schuster, M., Aboudhamad, W. N., Silversmith, R. E., and Bourret, R. B. (1998) *Mol. Microbiol. 27*, 1065−1075.
22. Welch, M., Oosawa, K., Aizawa, S.-I., and Eisenbach, M. (1994) *Biochemistry 33*, 10470−10476.
23. Blat, Y., and Eisenbach, M. (1994) *Biochemistry 33*, 902−906.
24. Nohaile, M., Kern, D., Wemmer, D. E., Stedman, K., and Kustu, S. (1997) *J. Mol. Biol. 273*, 299−316.
25. Welch, M., Oosawa, K., Aizawa, S.-I., and Eisenbach, M. (1993) *Proc. Natl. Acad. Sci. U.S.A. 90*, 8787−8791.
26. Zhu, X., Rebello, J., Matsumura, P., and Volz, K. (1997) *J. Biol. Chem. 272*, 5000−5006.
27. McEvoy, M., Hausrath, A. C., Randolph, G. B., Remington, S. J., and Dahlquist, F. W. (1998) *Proc. Natl. Acad. Sci. U.S.A. 95*, 7333−7338.
28. Welch, M., Chinardet, N., Mourey, L., Birck, C., and Samama, J.-P. (1998) *Nat. Struct. Biol. 5*, 25−29.
29. Li, J., Swanson, R. V., Simon, M. I., and Weis, R. M. (1995) *Biochemistry 34*, 14626−14636.
30. Birck, C., Mourey, L., Gouet, P., Fabry, B., Schumacher, J., Rousseau, P., Kahn, D., and Samama, J.-P. (1999) *Structure 7*, 1505−1515.
31. Lewis, R. J., Brannigan, J. A., Muchova, K., Barak, I., and Wilkinson, A. J. (1999) *J. Mol. Biol. 294*, 9−15.
32. Kern, D., Volkman, B. F., Luginbühl, P., Nohalle, M. J., Kustu, S., and Wemmer, D. E. (1999) *Nature 402*, 894−898.
33. Zhu, X., Volz, K., and Matsumura, P. (1997) *J. Biol. Chem. 272*, 23758−23764.
34. Alon, U., Camarena, L., Surette, M. G., Aguera y Arcas, B., Liu, Y., Leibler, S., and Stock, J. B. (1998) *EMBO J. 17*, 4238−4248.
35. Turner, L., Samuel, A. D., Stern, A. S., and Berg, H. C. (1999) *Biophys. J. 77*, 597−603.

BI9925524